(1.0–0.4 e Å^{-3}) corresponding to the hydrogen atoms, which were included in the subsequent refinement in geometrically idealized positions (C–H = 0.95 Å), and in addition overall isotropic thermal parameters were refined for the various types of hydrogen atoms. In the final cycles of refinement, a weighting scheme of the form $w = 1/(\sigma^2 F + pF^2)$ was employed where the final p parameter was 0.0032. Scattering factors used in the structure factor calculations were taken from ref 16 for non-hydrogen atoms and ref 17 for hydrogen atoms, and allowance was made for anomalous dispersion. A composite scattering factor curve with 0.5 occupancy for Pd and Pt was used for the disordered metal site. Refinement converged with $R = 0.044$ and $R_w = [\sum w\Delta^2/\sum wF_o^2]^{1/2} = 0.047$. A difference map calculated at the conclusion of the refinement showed electron density (~1.0 e Å^{-3}) in the vicinity of the metal atom and was insignificant.

(16) Cromer, D. T.; Mann, J. B. *Acta Crystallogr., Sect. A: Cryst. Phys., Diffr., Theor. Gen. Crystallogr.* **1968**, *A24*, 321.
(17) Stewart, R. F.; Davidson, E. R.; Simpson, W. T. *J. Chem. Phys.* **1965**, *42*, 3175.

The final fractional coordinates with estimated standard deviations are given in Table IV. Tables of hydrogen coordinates, anisotropic temperature factors and a structure factor listing have been deposited as supplementary material.

Acknowledgment. The continued financial support of the Natural Sciences and Engineering Research Council (to H.C.C. and G.F.) is gratefully acknowledged, as is the loan of platinum compounds by Johnson Matthey Ltd.

Registry No. $(PEt_3)ClPd(\mu\text{-}Cl)_2PtCl(PEt_3)$, 95387-53-4; $(PhMe_2P)Cl_2Pd(CH_2(pz)_2)PtCl_2(PPhMe_2)$, 103835-56-9; $(PEt_3)Cl_2Pt$(dim-c-Hx)$PtCl_2(PEt_3)$, 103835-57-0; $(PEt_3)Cl_2Pd$(dim-c-Hx)$PtCl_2(PEt_3)$, 103835-58-1; $(PPr_3)Cl_2Pd$(dim-c-Hx)$PtCl_2(PPr_3)$, 103835-59-2; $(PhMe_2P)Cl_2Pd$(dim-c-Hx)$PtCl_2(PPhMe_2)$, 103835-60-5; $(PhMe_2P)Cl_2Pd$(dim-*t*-Bu)$PtCl_2(PhMe_2P)$, 103835-61-6; $(PBu_3)Cl_2Pd$(dim-*t*-Bu)$PtCl_2(PBu_3)$, 103835-62-7.

Supplementary Material Available: Listings of anisotropic thermal parameters and calculated hydrogen atom coordinates (3 pages). Ordering information is given on any current masthead page.

Contribution from the Anorganisch-chemisches Institut, Technische Universität München, D-8046 Garching, West Germany, and Department of Chemistry, University of Houston, Houston, Texas 77004

Complexes with Phosphinomethanes and -methanides as Ligands. 10.[1] Formation, Structure, and Properties of $\{[(PMe_2CH_2PMe_2)(PMe_3)Co]_2PMe_2\}$, a Dinuclear, Odd-Electron Cobalt Complex of Formal Oxidation State Co_2^+. Electronic Structure of $[CoL_3]_2PR_2$ Radicals

Hans H. Karsch,*† Beatrix Milewski-Mahrla,† Jürgen O. Besenhard,† Peter Hofmann,*† Peter Stauffert,† and Thomas A. Albright‡

Received February 25, 1986

The paramagnetic, dinuclear complex $\{[(PMe_3)(Me_2PCH_2PMe_2)Co]_2PMe_2\}$ (**1**) is formed by P–C cleavage of a phosphine–Co(0) intermediate. Its solid-state structure was determined by X-ray diffraction methods (hexagonal, space group $P6_3/m$; $Z = 6$; $a = b = 16.285$ (7), $c = 19.296$ (6) Å; $R = 0.068$, $R_w = 0.062$, $w = 1/\sigma^2(F_o)$ for 130 refined parameters and 817 observables with $F_o \geq 4.0\sigma(F_o)$). Each cobalt atom binds four P atoms in a pseudotetrahedral environment. Two $Me_2PCH_2PMe_2$ groups and one PMe_2 group bridge the two cobalt atoms. The Co–Co distance is 2.603 (3) Å. The magnetic moment ($\mu_{eff} = 1.85$ (15) μ_B) is temperature-independent and corresponds to the presence of one unpaired electron. This is in accord with MO calculations (EHT), which show the delocalized electron to occupy a Co–Co antibonding (δ^*) and mainly metal centered SOMO. The results are compared with model calculations for the related complex $\{[(CO)_3Co]_2P[CH(SiMe_3)_2]_2\}$. In both cases actual geometries and ligand donor or acceptor properties of the Co_2L_6 skeleton have a pronounced effect upon energy and composition of the singly occupied molecular orbital. The molecular orbital results are in accord with cyclovoltammetric measurements, which reveal the existence of one reduction and three distinct oxidation steps for **1**, which are quasi-reversible. The diamagnetic monocation $\mathbf{1}^+$ is obtained by chemical oxidation of **1** and isolated as the BF_4^- salt. This complex cation exhibits fluxional behavior in solution (NMR), analogous to so-called molecular "A-frames".

Introduction

Much of the research on dinuclear complexes is dominated by the interest in metal–metal interactions[2] and, most recently, in so-called molecular "A-frames",[3,4] where two nearly planar metal centers are triply bridged by two diphosphino- (or diarsino-) methane ligands and an "apex" ligand like Cl, S, CO, SO_2, SR, PR_2, or others. Most of the A-frames described so far contain $Ph_2PCH_2PPh_2$ ligands. As an attractive alternative we have introduced $Me_2PCH_2PMe_2$[5] as a sterically less demanding ligand in metal complexes, which in addition improves their solubility properties.[5b] Therefore, a rapidly growing number of complexes with $Me_2PCH_2PMe_2$ ligands has now been described.[6] Normally the A-frames so far reported are even-electron-numbered, closed-shell diamagnetic compounds. In a preliminary communication we have briefly reported the formation and X-ray structure of the triply bridged dicobalt complex $\{[(PMe_3)(Me_2PCH_2PMe_2)Co]_2PMe_2\}$ (**1**),[6a] which formally seems related

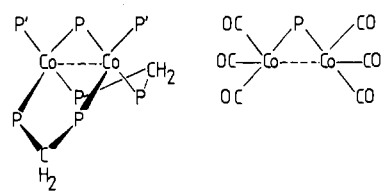

1 (P=PMe_2, P'=PMe_3) 2 (P=P[CH($SiMe_3$)$_2$]$_2$)

* To whom correspondence should be addressed: H.H.K., general chemistry and structure; P.H., MO calculations.
† Technische Universität München.
‡ University of Houston.

(1) Part 9: Karsch, H. H.; Müller, G.; Krüger, C. *J. Organomet. Chem.* **1984**, *272*, 195–212.
(2) Vahrenkamp, H. *Angew. Chem.* **1978**, *90*, 403–416; *Angew. Chem., Int. Ed. Engl.* **1978**, *17*, 379–392.
(3) (a) Kubiak, C. P.; Eisenberg, R. *J. Am. Chem. Soc.* **1977**, *99*, 6129–6131. (b) Kubiak, C. P.; Eisenberg, R. *Inorg. Chem.* **1980**, *19*, 2726–2732.
(4) Hoffmann, D. M.; Hoffmann, R. *Inorg. Chem.* **1981**, *20*, 3543–3555 and extensive literature cited therein.

0020-1669/86/1325-3811$01.50/0 © 1986 American Chemical Society

to the aforementioned A-frames. In contrast to the former, this complex is paramagnetic and has a pseudotetrahedral environment of the metal atoms. We expect this type of arrangement to be a quite common alternative to A-frames for such metal centers, which prefer tetrahedral geometries, as e.g. Co(0) or Co(I). We therefore will refer to this class of compounds, in analogy to A-frames,[3] as W-frames.

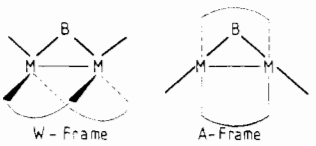

We now describe in detail formation, properties, X-ray structure, and magnetic and electrochemical properties as well as the electronic structure of **1**. In order to obtain a more profound understanding of the nature of this new class of dinuclear complexes, in particular to evaluate the role of the bridging diphosphine ligands in W-frames, MO calculations are included on the likewise paramagnetic, dinuclear complex $\{[(CO)_3Co]_2P[CH(SiMe_3)_2]_2\}$ (**2**), which has been independently synthesized by the Cowley group and which has been suggested to contain a related, but singly bridged, Co_2PR_2 framework.[7] In the case of **2**, the origin of the unpaired electron is evident from the introduction of the stable radical $P[CH(SiMe_3)_2]_2$[7] into the system, while in the case of **1**, this point needs further clarification.

Table I. Crystal Structure Data for **1**

formula	$C_{18}H_{52}Co_2P_7$
fw	603.3
cryst syst	hexagonal
space group	$P6_3/m$ (No. 176)
a, Å	16.285 (7)
b, Å	16.285 (7)
c, Å	19.926 (6)
V, Å^3	4431.7
Z	6
d_{calcd}, g/cm^3	1.356
μ(Mo Kα), cm^{-1}	15.0
T, °C	0
radiation	Mo Kα
λ, Å	0.71069
scan mode	ω
scan width (in ω), deg	1.0
scan rate (in ω), deg/min	0.9–29.3
scan range (in θ), deg	1–24
hkl range	+17,0 → −7,+22
no. of unique reflecns	1313
no. of obsd reflecns	817
ref params	130
R^a	0.068
$R_w{}^b$	0.062

$^a R = \sum(||F_o| - |F_c||)/\sum|F_o|$. $^b R_w = [\sum w(|F_o| - |F_c|)^2/\sum wF_o^2]^{1/2}$; $w = 1/\sigma^2(|F_o|)$.

Experimental Section

Materials and Physical Measurements. All experiments were carried out under a dry, oxygen-free dinitrogen atmosphere. Solvents were dried and distilled over sodium/potassium alloy. Starting materials, i.e. $[(Me_2PCH_2PMe_2)_2(PMe_3)]CoCl$,[6d] $(Me_3P)_3CoCl_2$,[8] $Me_2PCH_2PMe_2$,[5a] $(Me_3P)_4Co$,[9] and $LiPMe_2$[10] were prepared as described elsewhere. The ^1H NMR spectrum of 1^+ was run on a JEOL C-60 HL spectrometer and the ^{31}P NMR spectrum (36.43 MHz) on a Bruker HX 90 spectrometer. Chemical shifts are reported in ppm and coupling constants in Hz. Positive signs refer to low field. Melting points were determined in a sealed capillary by using a Büchi capillary melting point apparatus and are uncorrected. Mass spectra were recorded on a Varian MAT 311 A instrument. Solid-state susceptibility measurements were performed on a Princeton Applied Research magnetometer, Model 155, in the temperature range between 4.5 and 295 K. The resulting data were corrected for the diamagnetic contributions of the sample and the probe container. Cyclic voltammograms were recorded with a conventional setup, including a Pt-wire working electrode, surrounded by a cylindrical Pt counterelectrode. Potentials were measured vs. a saturated aqueous calomel electrode (SCE), which was separated from the working electrode by a fritted compartment filled with the nonaqueous electrolyte.

X-ray Data Collection and Structure Determination. Single crystals of $C_{18}H_{52}Co_2P_7$ (**1**) were grown from pentane at −78 °C. They crystallize in the hexagonal space group $P6_3/m$. A suitable single crystal was mounted in a Lindemann glass capillary on a four-circle diffractometer (Syntex $P2_1$). A total of 1313 independent reflections were measured at 273 K by using graphite-monochromatized Mo Kα radiation (λ = 0.71069 Å) and a scintillation counter (ω scan mode, $1 \leq \theta \leq 24°$). One standard reflection (002) was repeated after every 50 measured reflections and showed only random intensity fluctuations. After Lorentz and polarization corrections 817 structural factors with $F_o \geq 4.0\sigma(F_o)$ remained, which were used for all further calculations.[11]

The cobalt and phosphorus atoms were located by direct methods (Syntex-XTL). Subsequent difference Fourier synthesis gave the positions of the carbon atoms and, in part, of the hydrogen atoms. The remaining hydrogens were introduced at idealized calculated positions. Full-matrix least-squares refinement (non-H atoms anisotropic, H atoms fixed, 130 parameters, Syntex XTL) converged at $R = 0.068$, $R_w = 0.062$ ($w = 1/\sigma^2(F_o)$). Table I contains the crystal data; Table II lists the

(5) (a) Karsch, H. H.; Schmidbaur, H. *Z. Naturforsch., B: Anorg. Chem., Org. Chem.* **1977**, *32B*, 762–767. (b) Fild, N.; Heinze, J.; Krüger, W. *Chem. Ztg.* **1977**, *101*, 259–260.

(6) (a) Karsch, H. H.; Milewski-Mahrla, B. *Angew. Chem.* **1981**, *93*, 825–826; *Angew. Chem., Int. Ed. Engl.* **1981**, *20*, 814–815. (b) Karsch, H. H.; Schubert, U. *Z. Naturforsch., B: Anorg. Chem., Org. Chem.* **1982**, *37B*, 186–189. (c) Eberl, K.; Uedelhoven, W.; Karsch, H. H.; Kreissl, F. R. *Chem. Ber.* **1980**, *113*, 3377–3380. (d) Karsch, H. H. *Chem. Ber.* **1983**, *116*, 1643–1655. (e) Karsch, H. H. *Chem. Ber.* **1983**, *116*, 1656–1668. (f) Karsch, H. H. *Chem. Ber.* **1984**, *117*, 783–796. (g) Karsch, H. H. *Chem. Ber.* **1984**, *117*, 3123–3133. (h) Kullberg, M. L.; Kubiak, C. P. *Organometallics* **1984**, *3*, 632–634. (i) Ling, S. S. M.; Puddephatt, R. J.; Manojlovic-Muir, K. W. *Inorg. Chim. Acta* **1983**, *77*, L95–L96. (j) Tilley, T. D.; Andersen, R. A.; Zalkin, A. *Inorg. Chem.* **1983**, *22*, 856–859. (k) Bitterwolf, Th. E. *Polym. Mater. Sci. Eng.* **1983**, *49*, 368–371. (l) King, R. B.; Raghuveer, K. S. *Inorg. Chem.* **1984**, *23*, 2482–2491. (m) De Leeuw, G.; Field, J. S.; Haines, R. J.; McCulloch, B.; Meintjies, E.; Monberg, C.; Olivier, G. M.; Ramdial, P.; Sampson, C. N.; Sigwarth, B.; Steen, N. D.; Moodley, K. G. *J. Organomet. Chem.* **1984**, *275*, 99–111. (n) Manojlovic-Muir, L.; Muir, K. W.; Frew, A. A.; Ling, S. S. M.; Thomson, N. A.; Puddephatt, R. J. *Organometallics* **1984**, *3*, 1637–1645. (o) McLennan, A. J.; Puddephatt, R. J. *Organometallics* **1985**, *4*, 485–488. (p) Lee, K.-W.; Pennington, W. T.; Cordes, A. W.; Brown, T. L. *J. Am. Chem. Soc.* **1985**, *107*, 631–641. (q) Lee, K.-W.; Brown, T. L. *Organometallics* **1985**, *4*, 1025–1030, 1030–1036. (r) Wong, W. K.; Chin, K. W.; Wilkinson, G.; Howes, A. J.; Motevalli, M.; Hursthouse, M. B. *Polyhedron* **1985**, *4*, 603–614. (s) Wong, W. K.; Chin, K. W.; Wilkinson, G.; Motevalli, M.; Hursthouse, M. B. *Polyhedron* **1985**, *4*, 1231–1237. (t) Ling, S. S. M.; Jobe, I. R.; McLennan, A. J.; Manojlovic-Muir, L.; Muir, K. W.; Puddephatt, R. J. *J. Chem. Soc., Chem. Commun.* **1985**, 566–567. (u) Ling, S. S. M.; Jobe, I. R.; Manojlovic-Muir, L.; Muir, K. W.; Puddephatt, R. J. *Organometallics* **1985**, *4*, 1198–1202. (v) Azam, K. A.; Ferguson, G.; Ling, S. S. M.; Parvez, M., Puddephatt, R. J.; Srokowski, D. *Inorg. Chem.* **1985**, *24*, 2799–2802. (w) George, T. A.; Tisdale, R. C. *J. Am. Chem. Soc.* **1985**, *107*, 5157–5159. (x) Kullberg, M. L.; Lemke, F. R.; Powell, D. R.; Kubiak, C. P. *Inorg. Chem.* **1985**, *24*, 3589–3593. (y) Ling, S. S. M.; Payne, N. C.; Puddephatt, R. J. *Organometallics* **1985**, *4*, 1546–1550. (z) Lemke, F. R.; Kubiak, C. P. *J. Chem. Soc., Chem. Commun.* **1985**, 1729–1730. (aa) Ahmed, K. J.; Chisholm, M. H.; Folting, K.; Huffman, J. C. *Inorg. Chem.* **1985**, *24*, 4039–4044. (bb) Cotton, F. A.; Duraj, S. A.; Falvello, L. R.; Roth, W. J. *Inorg. Chem.* **1985**, *24*, 4389–4393. (cc) Tilset, M.; Vollhardt, K. P. C. *Organometallics* **1985**, *4*, 2230–2231. (dd) Pörschke, K. R.; Tsay, Y. H.; Krüger, C. *Inorg. Chem.* **1986**, *25*, 2097–2099. (ee) Collin, J.; Jossart, Ch.; Balavoine, G. *Organometallics* **1986**, *5*, 203–208. (ff) Manojlovic-Muir, L.; Ling, S. S. M.; Puddephatt, R. J. *J. Chem. Soc., Dalton Trans.* **1986**, 151–155. (gg) Jeffery, J. C.; Orpen, A. G.; Stone, F. G. A.; Went, M. J. *J. Chem. Soc., Dalton Trans.* **1986**, 173–186. (hh) Doherty, N. M.; Hogarth, G.; Knox, S. A. R.; Macpherson, K. A.; Melchior, F.; Orpen, A. G. *J. Chem. Soc., Chem. Commun.* **1986**, 540–542. (ii) Kullberg, M. L.; Kubiak, C. P. *Inorg. Chem.* **1986**, *25*, 26–30. (jj) Chakravarty, A. R.; Cotton, F. A.; Falvello, L. R. *Inorg. Chem.* **1986**, *25*, 214–219. (kk) Brandes, D. A.; Puddephatt, R. J. *Inorg. Chim. Acta* **1986**, *113*, 17–18. (ll) McLennon, A. J.; Puddephatt, R. J. *Organometallics* **1986**, *5*, 811–813.

(7) Cowley, A. H.; Kemp, R. A.; Wilburn, J. C. *J. Am. Chem. Soc.* **1982**, *104*, 331–332.

(8) Klein, H. F.; Karsch, H. H. *Chem. Ber.* **1976**, *109*, 1453–1464.

(9) Klein, H. F.; Karsch, H. H. *Chem. Ber.* **1975**, *108*, 944–955.

(10) Lundberg, K. L.; Rowa, H. R. J.; Miller, N. E. *Inorg. Chem.* **1969**, *8*, 1336–1340.

(11) Further details of the data collection may be found in: Wiberg, N.; Wagner, G.; Müller, G.; Riede, J. *J. Organomet. Chem.* **1984**, *271*, 381–391.

Table II. Atomic Coordinates and Thermal Parameters of the Non-Hydrogen Atoms for $\{[(PMe_3)(Me_2PCH_2PMe_2)Co]_2PMe_2\}$ (**1**)[a]

atom	G	x/a (s)	y/b (s)	z/c (s)	B_{11} (s)	B_{22} (s)	B_{33} (s)	B_{12} (s)	B_{13} (s)	B_{23} (s)
Co	1.0	0.0316 (2)	0.3566 (2)	0.1847 (1)	1.3 (1)	1.4 (1)	2.5 (1)	0.6 (1)	−0.1 (1)	−0.1 (1)
P1	1.0	−0.0749 (3)	0.3962 (3)	0.1759 (3)	2.6 (2)	3.2 (2)	2.8 (3)	2.2 (2)	−0.5 (2)	−0.3 (2)
P2	1.0	−0.0398 (3)	0.2036 (3)	0.1727 (3)	2.3 (2)	1.9 (2)	4.1 (3)	0.8 (2)	0.1 (2)	−0.6 (2)
P3	1.0	0.1096 (3)	0.4137 (3)	0.0935 (2)	2.5 (2)	2.7 (2)	2.6 (2)	1.2 (2)	0.1 (2)	0.3 (2)
P4	0.5	0.1484 (5)	0.3884 (4)	0.25 (Fp)	1.4 (3)	1.3 (3)	2.9 (3)	0.6 (3)	0.0 (Fp)	0.0 (Fp)
C1	0.5	−0.0393 (16)	0.1418 (15)	0.25 (Fp)	3.0 (1.4)	0.2 (1.0)	4.8 (1.3)	1.2 (9)	0.0 (Fp)	0.0 (Fp)
C2	1.0	0.0007 (16)	0.1461 (13)	0.1133 (10)	8.9 (1.6)	2.5 (1.0)	6.1 (1.3)	3.5 (1.0)	2.7 (1.1)	−1.0 (8)
C3	1.0	−0.1668 (14)	0.1387 (15)	0.1524 (12)	3.3 (1.1)	3.4 (1.1)	11.6 (1.8)	−0.1 (1.0)	4.9 (1.2)	−0.9 (1.3)
C4	0.5	0.2580 (17)	0.5098 (18)	0.25 (Fp)	1.6 (1.3)	4.0 (1.5)	2.9 (1.2)	0.4 (1.3)	0.0 (Fp)	0.0 (Fp)
C5	0.5	0.2099 (19)	0.3167 (18)	0.25 (Fp)	2.6 (1.5)	2.7 (1.4)	6.8 (1.9)	1.6 (1.3)	0.0 (Fp)	0.0 (Fp)
C6	1.0	−0.0347 (15)	0.5232 (13)	0.1636 (9)	7.4 (1.5)	3.9 (1.1)	3.5 (9)	3.6 (1.0)	0.5 (9)	1.0 (8)
C7	0.5	−0.1540 (18)	0.3646 (16)	0.25 (Fp)	4.2 (1.5)	3.5 (1.5)	2.3 (1.1)	2.9 (1.2)	0.0 (Fp)	0.0 (Fp)
C8	1.0	−0.1693 (14)	0.3537 (15)	0.1087 (10)	4.6 (1.2)	5.7 (1.3)	6.3 (1.4)	3.0 (1.1)	−3.2 (1.0)	−1.7 (11)
C9	1.0	0.1977 (14)	0.3827 (13)	0.0693 (9)	3.8 (1.1)	4.9 (1.2)	5.1 (1.0)	2.8 (1.1)	1.8 (1.0)	1.0 (1.0)
C10	1.0	0.0469 (14)	0.3880 (13)	0.0129 (9)	5.0 (1.3)	6.9 (1.5)	4.1 (1.0)	3.8 (1.2)	−0.9 (9.7)	−1.2 (9)
C11	1.0	0.1893 (16)	0.5443 (13)	0.0796 (11)	5.0 (1.4)	2.4 (1.0)	7.5 (1.5)	0.5 (9)	1.2 (1.1)	1.5 (9)

[a] The respective values for the hydrogen atoms are published as supplementary data; s = standard deviation, Fp = fixed parameter.

Table III. Important Distances and Angles for $\{[(PMe_3)(Me_2PCH_2PMe_2)Co]_2PMe_2\}$ (**1**)

	Distances (Å)		
Co–Co*	2.603 (3)	Co–P4	2.144 (7)
Co–P1	2.140 (7)	P1–C7	1.86 (2)
Co–P2	2.171 (5)	P2–C1	1.84 (1)
Co–P3	2.144 (5)		
	Angles (deg)		
Co–P4–Co*	74.8 (2)	P3–Co–P4	98.5 (2)
P1–C7–P1*	105.4 (11)	P1–Co–P2	106.7 (2)
P2–C1–P2*	113.5 (11)		

positional and thermal parameters for the non-hydrogen atoms. Selected bond distances and angles are collected in Table III.

Preparation of Compounds and Reactions. $\{[(Me_3P)(Me_2PCH_2PMe_2)Co]_2PMe_2\}$ (1). A. A solution of 1.5 g of $[(Me_3P)(Me_2PCH_2PMe_2)_2Co]Cl$[6d] (3.39 mmol) in tetrahydrofuran (40 mL) was warmed to 40 °C for 48 h. The green precipitate was filtered off, washed twice with pentane (30 mL), and identified analytically as $(PMe_3)_2(Me_2PCH_2PMe_2)CoCl_2$, dec pt 115 °C. Anal. Calcd for $C_{11}H_{32}Cl_2CoP_4$: C, 31.60; H, 7.71. Found: C, 31.16; H, 7.77. The mother liquor was evaporated to dryness, the residue dissolved in pentane (30 mL), and the solution filtered through a glass frit. The reddish brown solution was reduced to a small volume and slowly cooled to −78 °C. Red-brown crystals separated from the solution, which were washed at −20 °C with a small volume of pentane and dried in vacuo: dec pt 190 °C, yield 0.38 g (0.63 mmol); mass spectrum (EI) m/e (relative intensity) 603 (8, M^+), 527 (7, $M^+ - PMe_3$), 451 (16, $M^+ - 2PMe_3$), 390 (6, $[Co_2(Me_2PCH_2PMe_2)_2]^+$), 375 (27, $[Co_2(Me_2PCH_2PMe_2)(Me_2PCH_2PMe)]^+$), 315 (4, $[Co_2(PMe_2)(Me_2PCH_2PMe_2)]^+$), 301.6 (2, M^{2+}), 271 (5, $[Co(PMe_3)(Me_2PCH_2PMe_2)]^+$), 195 (5, $[Co(Me_2PCH_2PMe_2)]^+$), 136 (26, $Me_2PCH_2PMe_2^+$), 76 (83, PMe_3^+), 61 (100, PMe_2^+). Anal. Calcd for $C_{18}H_{52}Co_2P_7$: C, 35.85; H, 8.69; Co, 19.54. Found: C, 35.70; H, 8.71; Co, 19.47.

B. More directly **1** was also prepared by starting from $(Me_3P)_3CoCl$ and $Me_2PCH_2PMe_2$ without isolation of $[(PMe_3)(Me_2PCH_2PMe_2)Co]Cl$ as an intermediate; the procedure is analogous to method A (cf. ref 6d).

C. A 1.0-g portion of $(Me_3P)_4Co$ (2.75 mmol) and 560 mg of $Me_2PCH_2PMe_2$ (4.12 mmol) were heated under reflux in 30 mL of tetrahydrofuran for 10 h. The solvent was replaced by 20 mL of pentane; the further workup was as described in method A; yield 0.27 g (0.45 mmol).

D. The procedure was the same as in method C, but the addition of 0.19 g of $LiPMe_2$ (2.79 mmol) gave only traces of **1**.

E. To 0.8 g of $(Me_3P)_3CoCl_2$ (2.23 mmol) in 40 mL of tetrahydrofuran were added 0.5 g of $Me_2PCH_2PMe_2$ (3.68 mmol) and an excess of magnesium or 175 mg of potassium (4.48 mmol), respectively. The mixture was stirred for 24 h at room temperature. The workup follows that of method A; yield 130 and 110 mg of **1**, respectively.

F. Addition of $LiPMe_2$ to the mixture of method E (Mg reduction) gave only traces of **1**.

Oxidation of 1 with $AgBF_4$. A 1.2-g portion of **1** (1.99 mmol) and 425 mg of $AgBF_4$ (2.0 mmol) were stirred in tetrahydrofuran solution for 12 h. The solution was filtered through a glass frit and reduced to a small volume in vacuo. By addition of a small amount of ether, a dark brown, crystalline solid is precipitated. A total of 850 mg of product (62% of theory) is obtained; dec pt 120 °C. Anal. Calcd for $C_{18}H_{52}BCo_2F_4P_7$: C, 31.33; H, 7.60; Co, 17.08. Found: C, 31.04; H, 7.53; Co, 16.87.

Scheme I. Formation of $\{[L(Me_2PCH_2PMe_2)Co]_2PMe_2\}$ (**1**, L = PMe_3)

$$L_3CoCl + Me_2PCH_2PMe_2 \longrightarrow [L(Me_2PCH_2PMe_2)_2Co]Cl \xrightarrow[THF,\,40°C]{48\,h}$$

$$L_2(Me_2PCH_2PMe_2)_2CoCl_2 + \{[L(Me_2PCH_2PMe_2)Co]_2PMe_2\}$$

$$\underset{=}{1}$$

Results and Discussion

Formation of $\{[(PMe_3)(PMe_2CH_2PMe_2)Co]_2PMe_2\}$ (1). The unexpected formation of **1** first was observed during the attempted preparation of $[(PMe_3)(Me_2PCH_2PMe_2)_2Co]X$.[6d] Whereas in the case of X = PF_6 the product is indefinitely stable under ambient conditions, with X = Cl the complex decomposes at prolonged reaction times in tetrahydrofuran solutions (Scheme I).

Since the formation of $[(PMe_3)_2(Me_2PCH_2PMe_2)Co]Cl_2$ suggests a simple disproportionation pathway in this reaction, we initially assumed the second product, **1**, to be a cobalt(0) complex. Indeed, **1** is also obtained by a reaction according to the equation

$$(Me_3P)_4Co + 1.5\,Me_2PCH_2PMe_2 \xrightarrow[reflux]{THF} \underset{=}{1} + \text{unidentified products}$$

Furthermore, as expected for a phosphine complex of Co(0), **1** turned out to be paramagnetic and the mass spectrum (EI, 70 eV, 20 °C) showed the highest peak at m/e = 603, consistent with the formulation "$(Me_2PCH_2PMe_2)_4Co$". At closer sight, however, it turned out that further peaks at m/e = 527 and 451 are indicative of a subsequent loss of two PMe_3 units. Together with the elemental analysis, the correct formula for **1** could be derived and has been confirmed by an X-ray structure analysis (vide infra).

The main question then arose from the necessity of a P–C cleavage during the reaction course. It has been shown that this type of reaction is not uncommon in the Me_3P/Co(0) system.[12]

To get further insight into the reaction course, which is unusual in the sense that a dinuclear, paramagnetic complex is formed from even-electron-numbered reagents, we designed the reactions shown in Scheme II. The result of these reactions clearly requires that **1** be formed by a metal-centered process that is *not* promoted by added PMe_2^-. Hence, the decisive step, which generates the odd-electron-numbered, dimeric species, presumably is related to a homolytic P–C bond cleavage, generating CH_3 radicals. The alternative process, i.e. the formation of PMe_2 and CH_2PMe_2

(12) Klein, H. F. *Angew. Chem.* **1980**, *92*, 362–375; *Angew. Chem., Int. Ed. Engl.* **1980**, *19*, 362–375.

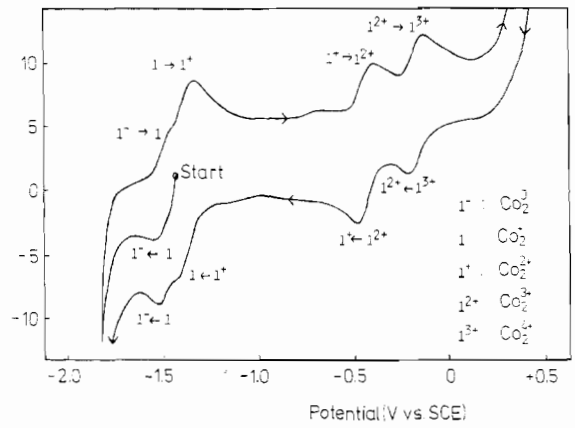

Figure 1. Cyclic voltammogram of ca. 2×10^{-3} M $\{[(PMe_3)(Me_2PCH_2PMe_2)Co]_2PMe_2\}$ (**1**, "Co_2^{+}") (in 0.5 M KPF_6/1,2-dimethoxyethane, room temperature, v = 100 mV s^{-1}, Pt working electrode (F_{geom} = ca. 0.025 cm^2)).

radicals from $Me_2PCH_2PMe_2$, seems unlikely because this should lead to a known type of complex (cf. ref 13). The fate of the proposed methyl radicals could not be determined, however.

Scheme II. Some Variations for the Preparation of **1**

$$(Me_3P)_3CoCl_2 + Me_2PCH_2PMe_2 + Mg \xrightarrow{THF} \mathbf{1} + \ldots$$

$$(Me_3P)_3CoCl_2 + Me_2PCH_2PMe_2 + K \xrightarrow{THF} \mathbf{1} + \ldots$$

$$(Me_3P)_3CoCl_2 + Me_2PCH_2PMe_2 + Mg + LiPMe_2 \xrightarrow{THF} \mathbf{1}\ (\text{traces}) + \ldots$$

$$(Me_3P)_4Co + Me_2PCH_2PMe_2 + {}^1/_2LiPMe_2 \xrightarrow{THF} \mathbf{1}\ (\text{traces}) + \ldots$$

Properties. $\{[(Me_3P)(Me_2PCH_2PMe_2)Co]_2PMe_2\}$ forms red-brown hexagon-shaped crystals (from pentane, dec pt >190 °C), readily soluble in hydrocarbon and ether solvents, but very sensitive to air and moisture. In solution (NMR) and in the solid, the complex is paramagnetic, with a temperature-independent (4.5–295 K) magnetic moment μ_{eff} = 1.85 (15) μ_B for the dimeric unit. This suggests a doublet ground state with one unpaired electron. A metal–metal bond order of 1.5 may therefore be derived from a qualitative electron-counting argument. More insight into the nature of **1** is obtained from its redox behavior. Complex **1** obviously can be electrochemically reduced to $\mathbf{1}^-$, corresponding to reduction of a "Co_2^{+}" system to "Co_2^{0}", now diamagnetic. This can be concluded from cyclic voltammograms (CV), which, moreover, demonstrate a sequence of redox processes between $\mathbf{1}^-$ and $\mathbf{1}^+$ ("Co_2^{0}" and "Co_2^{2+}") as shown in Figure 1.

When a cathodic CV sweep is started from the equilibrium potential of a freshly prepared solution of **1** ("Co_2^{+}"), only *one* reduction peak shows up, which, after potential reversal, is followed by two poorly resolved corresponding oxidation peaks. Under stationary conditions, i.e. after oxidation of **1** in a previous anodic sweep, there are also *two* reduction peaks which are just as poorly resolved as the corresponding oxidation peaks. We attribute this behavior to a reduction of **1** to $\mathbf{1}^-$ in the first cathodic sweep, followed by the reoxidation to **1** and a further oxidation to $\mathbf{1}^+$ in the first anodic sweep.

In continuous cycling experiments, as expected, the transitions $\mathbf{1}^-/\mathbf{1}$ and $\mathbf{1}/\mathbf{1}^+$ are observed in the anodic as well as in the cathodic sweeps. As judged from the dependence of the peak heights on the sweep rate v and from the separation of the anodic and cathodic peaks (E_{pc}, E_{pa}), which, however, can be determined only approximately, both reactions can be classified as quasi-reversible.

When the CV potential range is expanded into the positive direction, two additional quasi-reversible reactions are observed. We interpret these reactions as transitions between $\mathbf{1}^+$ and $\mathbf{1}^{2+}$ ("Co_2^{2+}" and "Co_2^{3+}") and between $\mathbf{1}^{2+}$ and $\mathbf{1}^{3+}$ ("Co_2^{3+}" and "Co_2^{4+}"), respectively. The potentials E ($E = {}^1/_2(E_{pa} + E_{pc})$) for the reactions $\mathbf{1}^-/\mathbf{1}$, $\mathbf{1}/\mathbf{1}^+$, $\mathbf{1}^+/\mathbf{1}^{2+}$, and $\mathbf{1}^{2+}/\mathbf{1}^{3+}$ are −1.48, −1.39, −0.44, and −0.17 V vs. SCE.

As expected, an ESR signal due to an unpaired electron can be observed for **1** in dilute solution. As in Cowley's compound **2** no coupling to the P nucleus of the μ-PMe_2 group is seen in the spectrum and the 15-line splitting pattern, poorly resolved, is indicative of coupling of the radical electron to two equivalent Co nuclei. Due to the extreme sensitivity of **1** in diluted solutions of the ESR experiments and due to the similarity of the observed spectrum of **1** to ESR spectra of mononuclear Co(0) phosphine complexes we hesitate, however, to present a full analysis of the ESR spectrum here. Its general appearance is in accord with the solid-state structure of **1** and with its orbital pattern (vide infra).

The redox behavior of **1** suggests the possibility of chemical reduction and oxidation without cleavage of the dimeric unit. Whereas **1** does not react with dihydrogen under ambient conditions (pentane, 25 °C, 1 atm of H_2, 60 h), reduction obviously is achieved by elemental potassium in tetrahydrofuran, as indicated by the color change of the solution from reddish brown to deep red. We were unsuccessful, however, in isolating the "Co_2^{0}" complex $\mathbf{1}^-$, since in the course of the workup, decomposition occurs.

Chemical oxidation of **1** is achieved by a reaction with $AgBF_4$. In an equimolar ratio, the "Co_2^{2+}" cation $\mathbf{1}^+$ may be isolated as dark brown crystals from tetrahydrofuran:

$$\{[(PMe_3)(Me_2PCH_2PMe_2)Co]_2PMe_2\} + AgBF_4 \xrightarrow[-Ag]{THF} \{[(PMe_3)(Me_2PCH_2PMe_2)Co]_2PMe_2\}^{\oplus}\ BF_4^{\ominus}$$

$$\underline{\mathbf{1}}^{\oplus}$$

As expected from the magnetic properties of **1**, this new complex $\mathbf{1}^+$ is diamagnetic. The $^{31}P\{^1H\}$ NMR spectrum (acetone-d_6, −100 °C, H_3PO_4 external reference) consists of a low-field signal for the bridging PMe_2 group ($\delta(PMe_2)$ = 148), split into a quintet due to coupling with the four (in solution time-averaged equivalent) ^{31}P nuclei of the $Me_2PCH_2PMe_2$ bridges ($^2J(PP)$ = 55 Hz), a broad but unresolved signal for these latter ^{31}P nuclei (δ-($Me_2PCH_2PMe_2$) = 13), and a sharp singlet for the PMe_3 groups ($\delta(PMe_3)$ = 5). When the sample is warmed (−70 °C), the PMe_2 and the $Me_2PCH_2PMe_2$ signals become rather broad, whereas the PMe_3 signal remains sharp at this temperature. This indicates the beginning of a dynamic process, which mainly involves the bridging $Me_2PCH_2PMe_2$ ligands. Further warming leads to a collapse of all signals due to the quadrupolar ^{59}Co nuclei.

In accordance with these observations, the $^1H\{^{31}P\}$ NMR spectrum of $\mathbf{1}^+$ is temperature dependent (Figure 2). At room temperature, single (slightly broadened) resonances are observed for all chemically different ^1H nuclei ($\delta(\mu\text{-}PMe_2)$ = 2.13; $\delta(PMe_3)$ = 1.59; $\delta(PMe_2$ ($Me_2PCH_2PMe_2$)) = 2.13; $\delta(CH_2)$ = 3.10). Cooling induces a high-field shift of all signals (−30 °C: $\Delta\delta$ = 0.15) but affects mainly the signals of the $Me_2PCH_2PMe_2$ ligand: the respective PMe_2 resonance is split into two singlets ($\Delta\delta$ = 0.86), and the CH_2 protons show an AB pattern ($^2J(HH)$ = 13.3 Hz) at −30 °C. The ^{31}P-coupled spectrum is qualitatively similar; the signals are slightly more broadened, but ^{31}P–^1H couplings are not resolved. This means that the expected inequivalence of these groups, due to a geometry that relates to the observed structure of the parent compound **1** in the solid state, is retained only at low temperature. The conformational (boat/chair) inequivalence of the $Me_2PCH_2PMe_2$ bridges, observed in the solid-state structure of **1**, is not met in the solution spectra of $\mathbf{1}^+$, probably due to rapid ring inversions. However, similar to the A-frame case, the PMe_2 and CH_2 protons of a given $Me_2PCH_2PMe_2$ ligand are still unisochronous, due to the different orientations of these groups relative to the "apex" (bridging PMe_2 group) of the W-frame. At higher temperature a still unknown dynamic process equilibrates these signals. This situation reminds one of the dynamic behavior of some "A-frames",[14] but the mechanism seems to be quite

(13) Klein, H. F.; Wenninger, J.; Schubert, W. *Z. Naturforsch., B: Anorg. Chem., Org. Chem.* **1979**, *34B*, 1391–1397.

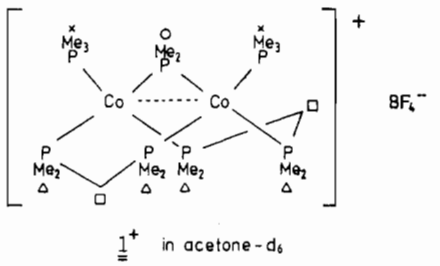

1^+ in acetone-d_6

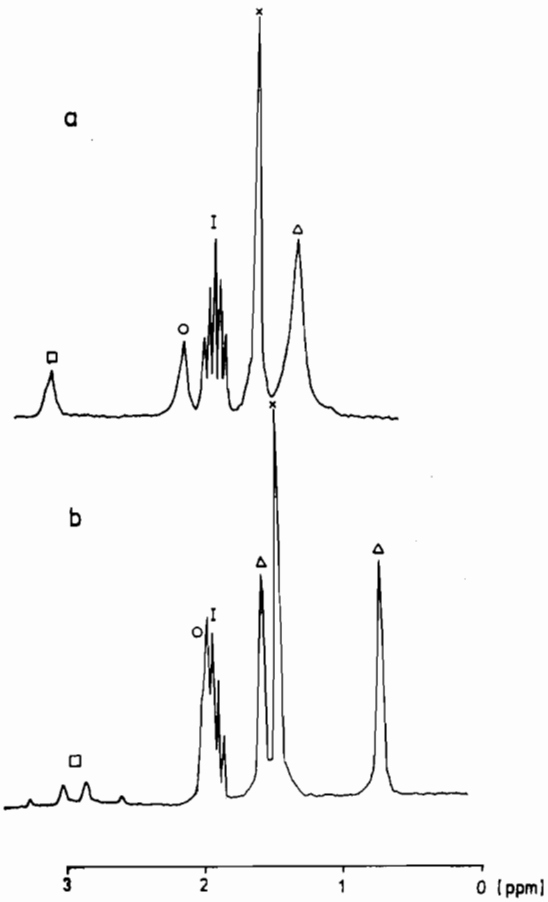

Figure 2. $^1H\{^{31}P\}$ NMR spectra of $\{[(PMe_3)(Me_2PCH_2PMe_2)Co]_2PMe_2\}BF_4$ ($\mathbf{1}^+$) (in acetone-d_6 (I), 60 MHz): (a) 25 °C; (b) −30 °C.

different. At present, we feel that the only reasonable explanation would imply a rapid dissociation/association cycle of the bridging $Me_2PCH_2PMe_2$ ligands. For $\mathbf{1}^+$ a value of $\Delta G^{\ddagger}_{-5°C} = 13.1$ kcal/mol can be derived for this dynamic process from ^1H NMR experiments. In this context, **1** and $\mathbf{1}^+$ seem to be ideal candidates for catalytic activity because of (i) facile substitution promoted by ligand dissociation, (ii) two metal sites held close together for cooperative binding, and (iii) an "electron reservoir" by reversible uptake and transfer of up to four electrons.

The high reactivity of **1** is indeed shown by the fast uptake of carbon monoxide in pentane solutions of **1** (1 atm of CO, 20 °C); the products could not yet be unambigously identified, however.

Molecular Structure of $\{[(PMe_3)(Me_2PCH_2PMe_2)Co]_2PMe_2\}$ (1). The X-ray structure determination of **1** reveals both cobalt atoms to be triply bridged by two $Me_2PCH_2PMe_2$ ligands and one PMe_2 group. An additional PMe_3 ligand completes the pseudotetrahedral coordination sphere of four phosphorus atoms for both of the cobalt atoms, and this constitutes the "W-frame" arrangement. The two methylene carbon atoms of the di-

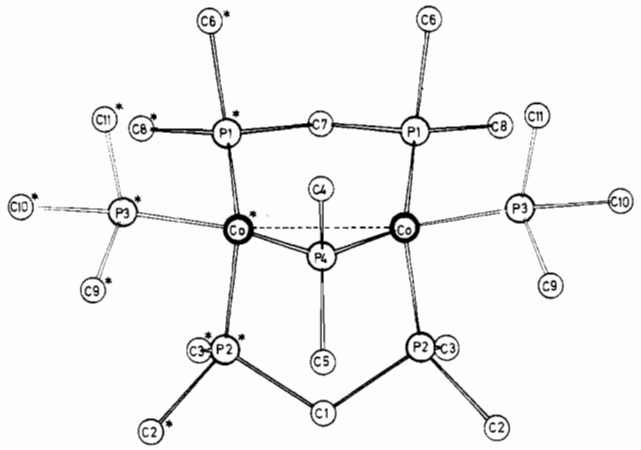

Figure 3. Drawing of the molecular structure of $\{[(PMe_3)(Me_2PCH_2PMe_2)Co]_2PMe_2\}$ (**1**) as obtained by X-ray structure determination.

phosphinomethane ligands, C1 and C7, and the bridging phosphido group, including atoms P1 and C4/C5, lie on a crystallographic mirror plane. This crystallographically imposed mirror symmetry is the most conspicuous feature of the molecular symmetry of **1**. In the following, all atoms marked by an asterisk (Figure 3 and Table III) are related to the unmarked ones by this molecular mirror plane. Angles and distances of the $Me_2PCH_2PMe_2$ ligands correspond well with the respective values of the free ligand.[15]

Together with the Co–P4–Co* fragment, each diphosphinomethane bridge forms a six-membered ring, which in one case (P1/C7/P1*/Co*/P4/Co) adopts a chair and in the other case (P2/C1/P2*/Co*/P4/Co) a boat conformation. This conformation can be predicted from molecular model examinations and may be attributed to steric interactions between the methyl groups at P1/P1*, P2/P2*, and P3/P3*. The angle between the planes Co,Co*,P1,P1* and Co,Co*,P2,P2* amounts to 107.4°. All the angles at phosphorus and the P–C and Co–P bond lengths (Table III) are in the expected range. Exceptions are as follows. The angle Co–P4–Co* (74.8 (2)°) is noticeably smaller than 90°. Remarkably, the respective value in complex **3** (74.9°)[16] is virtually

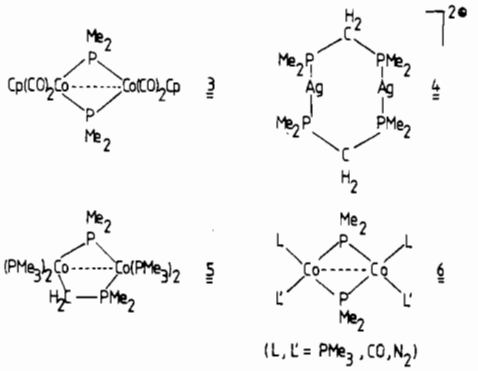

identical. On the other hand, both the angles at the methylene carbon atoms C1 and C7 are smaller than in the $Me_2PCH_2PMe_2$-bridged complex cation **4** (117.6°).[6b] The two angles are quite different (114 (1) and 105 (1)°), however, although the large standard deviations suggest that not too much emphasis should be attributed to this difference. The smaller P–C–P angles are almost certainly a consequence of the rather short Co–Co* distance of 2.603 (3) Å, which is much less than d(Ag–Ag) in **4** (3.04 Å).[6b] This compares to d(Co–Co) in **3** (2.59 Å), which has been assigned to a Co–Co bond near the lower limit for phosphido-bridged dinuclear cobalt complexes.[16] This distance might even be shorter, did not the methyl groups on the phosphorus

(14) For a recent discussion see: Puddephatt, R. J.; Azam, K. A.; Hill, R. H.; Brown, M. P.; Nelson, C. D.; Moulding, K. P.; Seddon, R. P.; Grossel, M. C. *J. Am. Chem. Soc.* **1983**, *105*, 5642–5646.

(15) Rankin, D. W. H.; Robertson, H. E.; Karsch, H. H. *J. Mol. Struct.* **1981**, *77*, 121–126.

(16) Keller, E.; Vahrenkamp, H. *Z. Naturforsch., B: Anorg. Chem., Org. Chem.* **1978**, *33B*, 537–541.

atoms exert a mutual repulsive steric interaction and hence prevent further approach of the cobalt atoms. Due to the different geometry and overall number of electrons in **3** ("Co_2^{4+}"), the comparison with **1** should be taken with care, however.

In complex **5**,[13] a much stronger Co–Co interaction ("four-electron bonding") is indicated by the shorter Co–Co distance (2.43 Å) and a smaller angle Co–P–Co (68.6°), however. Similar values are reported for **6**.[17]

Thus the metal–metal bonding interaction in the "Co_2^{+}" complex **1** is clearly weaker than in the likewise pseudotetrahedral "Co_2^{2+}" complexes **5** and **6**. This seems to indicate that the "extra" electron in **1** resides in a metal–metal antibonding orbital, as indeed will be shown to be the case from MO calculations. From this point of view one would expect the complex cation $\mathbf{1}^+$ to have a higher degree of Co–Co bonding than **1**.

On the other hand, as pointed out by Hoffmann et al.,[4] molecular A-frames like **7** (denoted "d^8–d^{8}") should not have a bonding metal–metal interaction. A complex of structure **8**

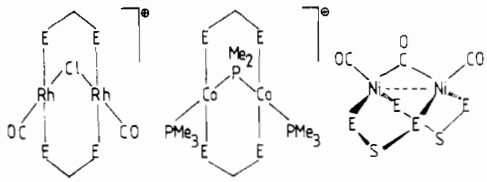

7 (E = PPh_2) **8** (E = PMe_2) **9** (E = $P(CF_3)_2$)

(A-frame, i.e. square-planar Co metal centers) would belong to the same category of complexes and might also be an adequate alternative for $\mathbf{1}^+$ (likewise "d^8–d^{8}"). However, in contrast to the case for the heavier analogues rhodium and iridium, known tetracoordinate Co^+ (d^8) as well as Co(0) (d^9) complexes adopt a tetrahedral configuration throughout[12] and, hence, the conformation of $\mathbf{1}^+$ almost certainly is analogous to **1**. Interestingly, complex **9** ("d^9–d^{9}") has pseudotetrahedral Ni centers,[18] and this very much resembles the actual geometry of **1** ("d^9–d^{8}"), i.e., belongs to the same class of W-frames.

The structural details and comparisons described above, the interesting redox behavior, and the presence of one unpaired electron in **1** and in the related system **2**, as well as the reported ESR properties of the latter, prompted us to study the electronic structure of these unique $Co_2L_6PR_2$ compounds in more detail. This forms part of a general theoretical investigation of alkylidene, ML_2, etc. bridged transition-metal dimers by us and other workers.[19]

Electronic Structure of $\{[(PMe_3)(Me_2PCH_2PMe_2)Co]_2PMe_2\}$ (1) and of $\{[(CO)_3Co]_2P[CH(SiMe_3)_2]_2\}$ (2). MO Model Calculations. MO model calculations for the two simplified "parent" systems of **1** and **2**, i.e. for **10** and **11**, were performed to get a somewhat clearer picture of the electronic structure of such $[L_3Co]_2PR_2$ type radicals. For **11** the replacement of the bulky

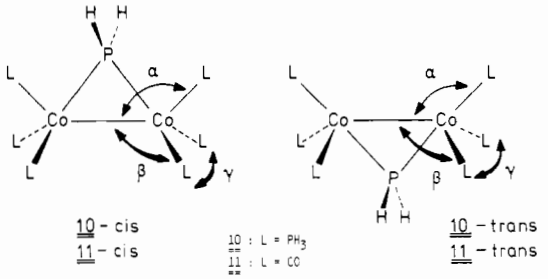

$CH(SiMe_3)_2$ groups by H should not affect the basic electronic structure; neither should the replacement of Me by H in **10** be crucial. Substituting the two chelating diphosphine ligands by four monodentate phosphine groups, however, will allow us to say something about the influence of chelation upon electronic structure and stability. It seems conceivable that steric constraints imposed by chelating ligands play a role for **1**. This question will be unraveled by model calculations for **10** with an enforced PH_3 ligand arrangement analogous to that found for the P centers in **1** as well as by calculations for $\{[(PH_3)(H_2PCH_2PH_2)Co]_2PH_2\}$, the actual model of **1** with chelate ligands and only CH_3 replaced by H. Of particular interest of course are the nature and the relative energies of the molecular orbitals housing the unpaired electron in **1** and **2** as well as the metal–metal interaction in these compounds. The consequence of phosphine vs. CO ligands has to be probed in this context.

All calculations employed the extended Hückel method,[20] with computational and geometric details (as far as not described in the text) provided in the Appendix.

For **10** as well as for **2** and its PH_2 model different idealized geometric arrangements for the PR_2 (PH_2) bridge with respect to the Co_2L_6 fragment are possible, as indicated by the cis and trans forms of **10** and **11** (C_{2v} symmetry throughout). As no structure determination for **2** has been hitherto reported, an investigation of **11**-cis vs. **11**-trans by theoretical methods seems challenging and is of course related to the question of stereochemical nonrigidity (e.g. CoL_3 group rotations). The presence in **1** of two chelating bidentate $Me_2PCH_2PMe_2$ ligands imposes a geometry near that of **10**-cis (viz. Figure 3), whereas in a nonchelated system as in **10** or in its analogues no a priori choice between **10**-cis and **10**-trans is obvious, albeit **10**-trans may look better for steric reasons. We therefore first performed geometry optimizations for **10**-cis and **10**-trans, independently varying angles α, β, and γ on each metal center, keeping the Co_2P core fixed and retaining overall C_{2v} symmetry with constant bond lengths. The lowest energy structure is **10**-trans, with $\alpha = 100°$, $\beta = 116.5°$, and $\gamma = 122°$. The minimum for **10**-cis is found to be 16.8 kcal/mol higher in energy, with $\alpha = 145°$, $\beta = 105°$, and $\gamma = 109°$. Note that the latter structure with its "cis" μ-PH_2 position as in **1** displays an overall $Co_2(PH_3)_6$ fragment geometry, which is still quite different from the geometry of the $Co_2(PMe_3)_2(Me_2PCH_2PMe_2)_2$ fragment in **1** with respect to its Co_2P_6 skeleton. For both **10**-cis and **10**-trans minimum geometries the CoL_3 groups relax in such a way as to reorient their pseudothreefold axis away from the other metal toward the PH_2 bridge, thus removing repulsion with this group and improving Co–μ-PH_2 bonding. What is more interesting, however, is that the calculations show only very weak Co–Co bonding for both minimum

(17) Jones, R. A.; Stuart, A. L.; Atwood, J. L.; Hunter, W. E. *Organometallics* **1983**, *2*, 1437–1441.

(18) Einspahr, H.; Donohue, J. *Inorg. Chem.* **1974**, *13*, 1839–1843. For the effect of a μ-CO as compared to a μ-PR_2 group see text.

(19) (a) Hofmann, P. *Angew. Chem.* **1979**, *91*, 591–593; *Angew. Chem., Int. Ed. Engl.* **1979**, *18*, 554–556. (b) Pinhas, A. R.; Albright, T. A.; Hofmann, P.; Hoffmann, R. *Helv. Chim. Acta* **1980**, *63*, 29–49. (c) Calabro, D. C.; Lichtenberger, D. L.; Herrmann, W. A. *J. Am. Chem. Soc.* **1981**, *103*, 6852–6855. (d) Viles, J.; Fehlner, T. P. *J. Electron Spectrosc. Relat. Phenom.* **1981**, *24*, 215–219. (e) Van Dam, H.; Stufkens, D. J.; Oskam, A.; Doran, M.; Hillier, I. H. *J. Electron Spectrosc. Relat. Phenom.* **1980**, *21*, 47–55. (f) Dedieu, A.; Hoffmann, R. *J. Am. Chem. Soc.* **1978**, *100*, 2074–2079. (g) Norman, J. G., Jr.; Gmur, D. J. *J. Am. Chem. Soc.* **1977**, *99*, 1446–1450. (h) Benard, M. *Inorg. Chem.* **1979**, *18*, 2782–2785. (i) Granozzi, G.; Tondello, E.; Casarin, M.; Afo, D. *Inorg. Chim. Acta* **1981**, *48*, 73–76. (j) Benard, M. *J. Am. Chem. Soc.* **1978**, *100*, 7740–7742. (k) D'Errico, J. J.; Curtis, M. D. *J. Am. Chem. Soc.* **1983**, *105*, 4479–4480. (l) Pinhas, A. R.; Hoffmann, R. *Inorg. Chem.* **1979**, *18*, 654–658. (m) Burdett, J. K. *J. Chem. Soc., Dalton Trans.* **1977**, 423–428. (n) Hay, P. J.; Thibeault, J. C.; Hoffmann, R. *J. Am. Chem. Soc.* **1975**, *97*, 4884–4899. (o) Dudeney, N.; Kirchner, O. N.; Green, J. C.; Maitlis, P. M. *J. Chem. Soc., Dalton Trans.* **1984**, 1877–1882. (p) Dudeney, N.; Green, J. C.; Kirchner, O. N.; Smallwood, F. S. J. *J. Chem. Soc., Dalton Trans.* **1984**, 1883–1887. (q) Morris-Sherwood, B.; Powell, C. B.; Hall, M. B. *J. Am. Chem. Soc.* **1984**, *106*, 5079–5083. (r) Kang, S.-K.; Albright, T. A.; Wright, T. C.; Jones, R. A. *Organometallics* **1985**, *4*, 666–675. (s) Summerville, R. H.; Hoffmann, R. *J. Am. Chem. Soc.* **1976**, *98*, 7240–7254. (t) Teo, B. K.; Hall, M. B.; Fenske, R. F.; Dahl, L. F. *Inorg. Chem.* **1975**, *14*, 3103–3117. (u) Benard, M.; Dedieu, A.; Nakamura, S. *Nouv. J. Chim.* **1984**, *8*, 149–157. (v) For theoretical studies of monobridged M_2L_6 fragments see ref 21 and 25.

(20) Hoffmann, R. *J. Chem. Phys.* **1963**, *39*, 1397–1412. Hoffmann, R.; Lipscomb, W. N. *J. Chem. Phys.* **1962**, *36*, 2179–2189. The atomic parameters used are either standard ones (C, H, O) or are taken from earlier work (Co, P); for details see Table IV.

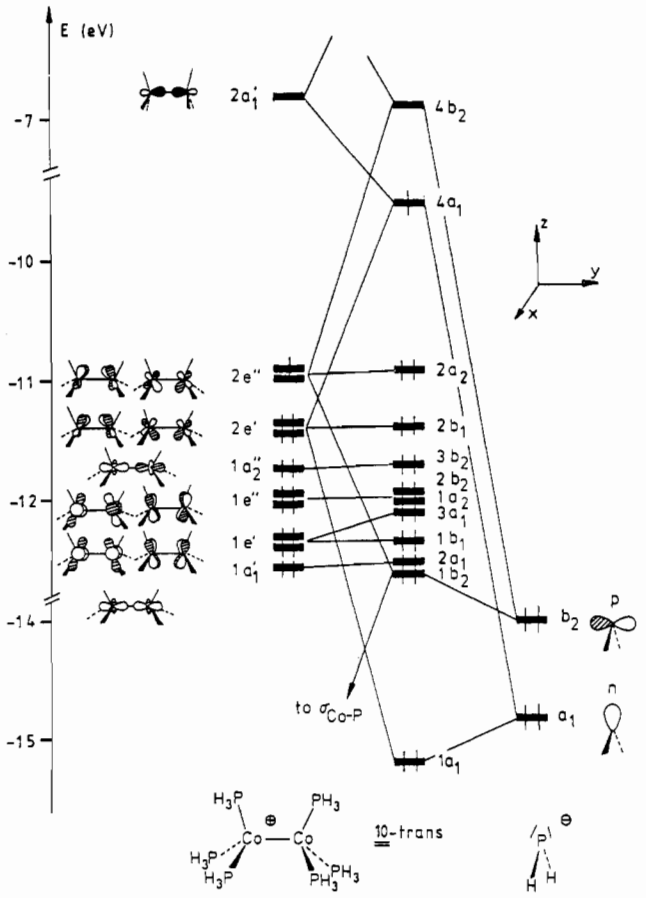

Figure 4. Interaction diagram between a D_{3h} $Co_2(PH_3)_6^+$ fragment and a PH_2^- group for the **10**-trans geometry, $\alpha = \beta = \gamma = 109.5°$. Note that the dimetal fragment MOs have been labeled in D_{3h} symmetry and the molecule as well as the PH_2 fragment MOs in C_{2v} symmetry. Thus, two different coordinate systems apply. That for the molecule is shown. The antibonding counterpart of $2a_1'$, which has a_2'' symmetry, is too high in energy to appear in this figure.

structures. The computed overlap population n_{Co-Co} is only 0.079 in **10**-trans and 0.082 in **10**-cis. An inspection of the MO structure of both cases reveals that this corresponds to a formal bond order of only 0.5 between the metal centers, in contrast to the aforementioned simple electron-counting expectations of a 1.5 bond order, and this seems quite incompatible with the observed structure, stability, and chemistry of **1**. It is the unpaired electron alone, residing in a Co–Co bonding MO of a_1 symmetry, that brings about the minute net bonding interaction between the metals in **10**, and we now proceed to analyze this unexpected result, which, as will be shown below, is in sharp contrast to the electronic structure of the chelated diphosphine system and the hexacarbonyl case **11**.

It is most informative to look at these $L_6Co_2PR_2$ ring systems in terms of the dimetal fragment Co_2L_6, interacting with a bridging PR_2 group, either taking both subunits neutral with one unpaired electron from $PR_2^•$ or considering an open-shell (17e) $Co_2L_6^+$ (d^8–d^9) and a phosphido bridge PR_2^-. The valence orbitals of both types of groups are well-known, and those of a Co_2L_6 building block are derived most conveniently from the levels of two conical CoL_3 groups.[21] Let us therefore start out from the "unrelaxed" structure **10**-trans, containing a D_{3h} $Co_2(PH_3)_6$ unit (with "tetrahedral" CoL_3 groups, $\alpha = \beta = \gamma = 109.5°$) bound to a PH_2 bridge. Figure 4 on the left side shows the valence MOs of the D_{3h} $Co_2(PH_3)_6^+$ fragment of "unrelaxed" **10**-trans, as they are derived from the levels of two $Co(PH_3)_3$ fragments[22] and as they

(21) Thorn, D. L.; Hoffmann, R. *Inorg. Chem.* **1978**, *17*, 126–140.

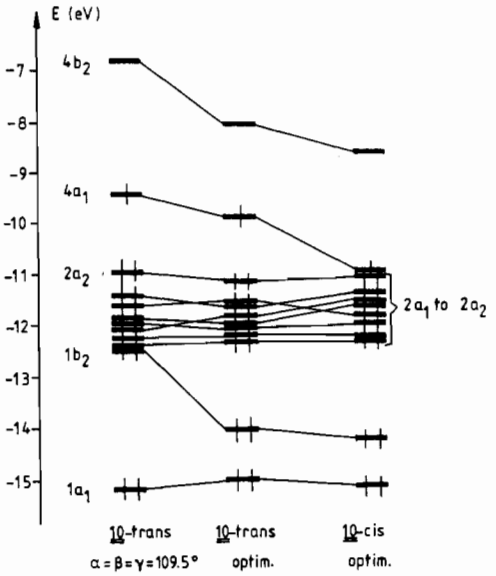

Figure 5. Valence MO energy changes on going from **10**-trans with a D_{3h} dimetal fragment to optimized **10**-trans. On the right side the MO energies of optimized **10**-cis are also shown.

evolve from the calculations. Above a nest of 10 d-block levels, $1a_1'$ to $2e''$, close in energy to each other, lies $2a_1'$, derived from the sp hybrids of CoL_3, which is Co–Co bonding and is rather high in energy. Due to the well-understood "tilt" of ML_3 1e and 2e levels,[23] ($x^2 - y^2$, xy) and (xz, yz) character are strongly mixed in the $Co_2(PH_3)_6$ levels of e′ and e″ symmetry. This is indicated qualitatively along with the predominant σ, π, or δ bonding/antibonding character in Figure 4. On the right side of the figure the two relevant valence levels of PH_2^- are given, the n-type lone pair of a_1 symmetry and above it the filled level of b_2 type, a pure 3p level of phosphorus. The molecular orbitals of **10**-trans (D_{3h} Co_2L_6) then consist of eight essentially unaffected d AO linear combinations and only two levels of the Co_2L_6 $1a_1'$ to $2e''$ block interact strongly with PH_2^- MOs. $n(a_1)$ of PH_2^- interacts with the appropriate member of 2e′, forming molecular orbitals $1a_1$ and $4a_1$ of the complex. $1a_1$ at low energy holds two of the four μ-PH_2–Co bonding electrons; $4a_1$, mainly localized in the metal fragment, houses the unpaired electron and mixes into itself $2a_1'$ of $Co_2(PH_3)_6$ in a bonding way. This is shown in **12** in a qualitative sense. The second dominant interaction is between the p-type lone pair b_2 of PH_2^- and the $2e''$ component of equivalent symmetry. Their antibonding combination $4b_2$ lies at high energy and is the LUMO of the system. Into the bonding linear combination $1b_2$ two low-lying $Co_2(PH_3)_6$ MOs, not shown in Figure 4, mix in from below with an antibonding phase (as shown in **13** for one of them), with $1b_2$ kept at very high energy just below the d block.

In a sense MOs $1a_1$, $1b_2$ and $4a_1$, $4b_2$ are Walsh-type bonding and antibonding orbitals, respectively, of the Co_2P three-membered ring. The high energy of $1b_2$ simply reflects severe mutual steric repulsion of Co–PH_2 and Co–PH_3 bonding electrons due to the chosen fixed geometry of **10**-trans. For **10**-cis with $\alpha = \beta = \gamma$

(22) For some other treatments of conical ML_3 fragments see also: (a) Elian, M.; Hoffmann, R. *Inorg. Chem.* **1975**, *14*, 1058–1076. (b) Elian, M.; Chen, M. M. L.; Mingos, D. M. P.; Hoffmann, R. *Inorg. Chem.* **1976**, *15*, 1148–1155. (c) Albright, T. A.; Hofmann, P.; Hoffmann, R. *J. Am. Chem. Soc.* **1977**, *99*, 7546–7557. (d) Albright, T. A.; Hoffmann, R. *J. Am. Chem. Soc.* **1978**, *100*, 7736–7738. (e) Dedieu, A.; Albright, T. A.; Hoffmann, R. *J. Am. Chem. Soc.* **1979**, *101*, 3141–3151. (f) Summerville, R. H.; Hoffmann, R. *J. Am. Chem. Soc.* **1979**, *101*, 3821–3831. (g) Goldberg, K. I.; Hoffman, D. M.; Hoffmann, R. *Inorg. Chem.* **1982**, *21*, 3863–3868. (h) Hoffmann, R. *Angew. Chem.* **1982**, *94*, 725–739; *Angew. Chem., Int. Ed. Engl.* **1982**, *21*, 711–724. (i) Albright, T. A.; Burdett, J. K.; Whangbo, M. H. *Orbital Interactions in Chemistry*; Wiley: New York, 1985.

(23) This phenomenon has been analyzed in ref 22c as a function of L and of and the pyramidality of ML_3. See also the treatment of $M(PH_3)_3$ and $M_2(PH_3)_6$ in: Di Vaira, M.; Sacconi, L. *Angew. Chem.* **1982**, *94*, 338–351; *Angew. Chem., Int. Ed. Engl.* **1982**, *21*, 330–342.

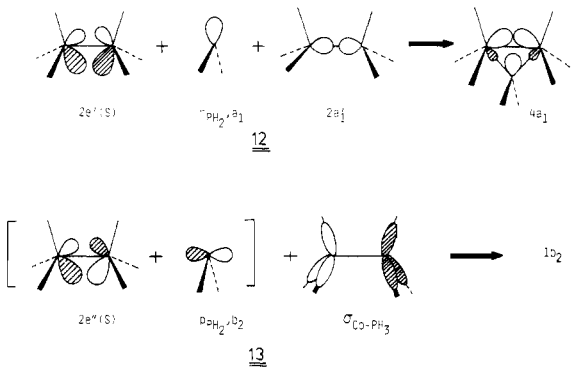

12

13

= 109.5°, "unrelaxed", but with a "cis" arrangement of the μ-PH_2 group, this type of repulsion is even more pronounced and the analogous level is found at the upper end of the d levels, the total energy being about 4 eV higher. If the geometries of **10**-trans and **10**-cis are optimized, relaxation leads to the above-mentioned minimum structures and practically all of the driving force toward the optimum values of α, β, and γ stems from the gain in energy of $1b_2$. In Figure 5 the valence energy level changes for relaxation from the geometry of Figure 4 to the minimum of **10**-trans are shown.

A similar picture holds, of course, if **10**-cis with a D_{3h} Co_2P_6 fragment geometry is distorting to its minimum energy structure, and on the right side of Figure 5 the MOs of optimized **10**-cis (less stable) are given for comparison. Note that for **10**-cis the singly occupied MO $4a_1$ is stabilized more upon relaxation of the Co_2P_6 skeleton than for **10**-trans—this will be important with respect to the chelated phosphine system below. For both cases energy changes due to geometry relaxation are also occurring within the nest of lower lying levels; their origin can be easily visualized from the wave functions qualitatively shown in Figure 4 and from Co–Co or Co–PH_2 overlap changes in the course of going toward the minimum structures of **10**-cis and **10**-trans.

With respect to the overall electronic structure of **10**-cis and **10**-trans as models for real systems with monodentate phosphines, it is most important that, for both conformations, and in particular for the more stable one **10**-trans, the unpaired electron is in MO $4a_1$ above the d block, while the next lower level $2a_2$ of mixed π^*/δ^* type is doubly occupied. For this MO pattern, the unpaired electron in $4a_1$ alone contributes to Co–Co bonding, because metal–metal bonding and antibonding contributions of σ, π, and γ type from the other metal valence electrons cancel.

The electronic structure computed for such $Co_2L_6(\mu\text{-}PH_2)$ molecules with monodentate phosphine ligands is also incompatible with the lack of any observable ESR coupling of the unpaired electron in compound **1** to the μ-P nucleus (MO $4a_1$ carries lone-pair character and therefore some 3s contribution of phosphorus in the wave function). Moreover, the calculations suggest that analogues of **1** with only monodentate phosphines as ligands should not be stable. This is in accord with our unsuccessful efforts to get access to such complexes with various types of PR_3 ligands replacing bis(dimethylphosphino)methane.

On the basis of the results for unchelated **10**-cis and **10**-trans minimum structures, we next performed model calculations for **10**-cis with a fixed set of the angles α, β, and γ, chosen to create a P_6 ligand arrangement as close as possible to that of **1**. For these appropriate angles α = 150°, β = 93.5°, and γ = 106.6° the electronic structure of **10**-cis is altered drastically. Actually **1** only has C_s symmetry, because of the two chelate rings one adopts a chair conformation and the other is boat shaped (cf. Figure 3). So for the P_6 ligand arrangement modeling **1**, α and γ are taken from the structure, β is an average value, and overall C_{2v} symmetry is preserved. Figure 6 displays the valence orbital energy changes that occur if **10**-cis with an optimized fragment $Co_2(PH_3)_6$ is distorted to a metal fragment sawhorse structure (C_{2v}) with the above-mentioned α, β, and γ values modeling **1**. Note that γ is 2.4° smaller, α is 5° larger, and β is 11.5° smaller than found for the optimized geometry of **10**-cis; the total energy is of course much higher than in the latter, due to an increase of steric repulsion between ligands. For the fixed "chelate-model" geometry, however, the two highest occupied molecular orbitals of a_1 and a_2 symmetry reverse their energetic ordering. $4a_1$ becomes stabilized further, correlating with $4a_1$ on the right side. So $2a_2$, nearly unaffected by enforcement of the chelate-type P_6 environment, takes over the role of the singly occupied MO. $4a_1$ now holds two electrons. The energetic descent of $4a_1$ is again easily understood in terms of Co_2P_6 and PH_2 fragment MOs. For a D_{3h} Co_2P_6 frame (cf. Figure 4) $4a_1$ is the antibonding linear combination of the symmetric 2e′ component of $Co_2(PH_3)_6$ and of $n(a_1)$ of PH_2, mixing into itself $2a_1'$ (σ_{sp}) of the dimetal fragment weakly from above, analogous to the situation shown in **12**. The distorted geometry modeling **1** rehybridizes and reorients the two metal-based levels as indicated in **14** and **15**.

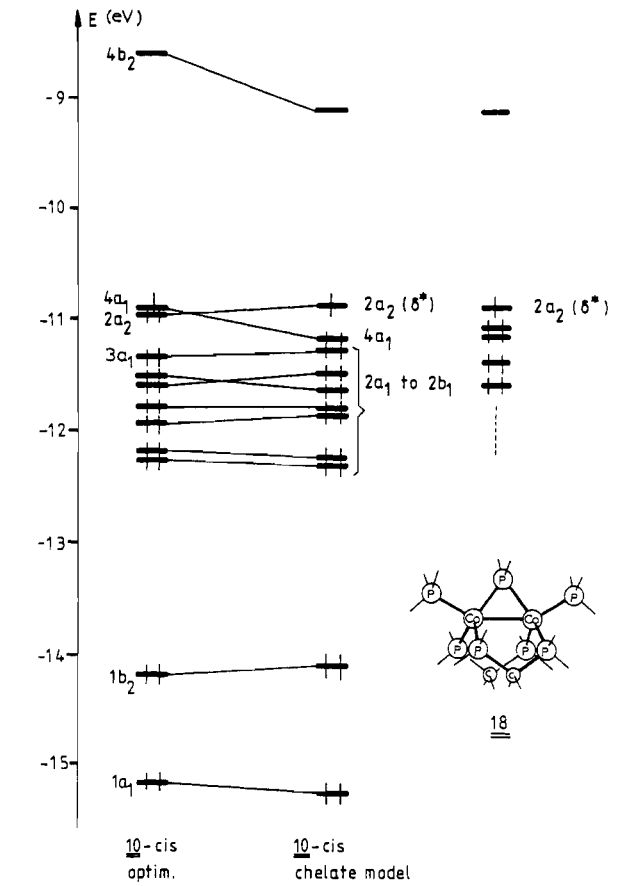

18

Figure 6. Valence MO energy changes for distorting **10**-cis (optimized) to **10**-cis with a geometry modeling **1**.

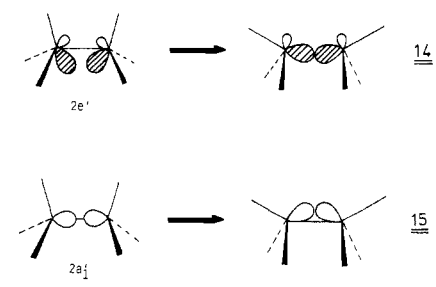

14

15

As a consequence the antibonding interaction of $n(a_1)$ of PH_2 with **14** is diminished because of reduced mutual overlap.[24] Actually **14** becomes a practically metal based level ($3a_1$). A lower lying Co_2P_6 MO, of δ type, shown schematically in **16** and localized in $3a_1$ on the left of the structure, now interacts with $n(a_1)$ of PH_2. It becomes the main contributor to $4a_1$ on the right of the structure

(24) $\langle 2e_s'/n(a_1)\rangle$ = 0.1573 for **10**-cis with a D_{3h} Co_2P_6 fragment vs. $\langle 14/n(a_1)\rangle$ = 0.0347 for the **10**-cis chelate model, and $\langle 2a_1'/n(a_1)\rangle$ = 0.4313 for **10**-cis with a D_{3h} Co_2P_6 fragment vs. $\langle 15/n(a_1)\rangle$ = 0.552 for the **10**-cis chelate model.

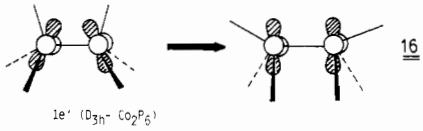

16

into which **15** can also mix better in a bonding way from above due to its increased overlap[24] with n(a_1) of PH_2.

As $4a_1$ emerges below the $2a_2$ level, two electrons now are in this Co–Co bonding MO, and the unpaired electron resides in $2a_2$, which, again as a consequence of the enforced geometry analogues to that of **1**, has turned into a purely δ^*-type MO, shown in **17**.

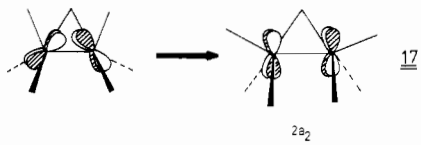

17

The geometry-induced level inversions of Figure 6 lead to a pronounced increase of the Co–Co reduced overlap population for going from the D_{3h} Co_2P_6 system or the **10**-cis geometric minimum (0.082) to the chelate model (0.133), consistent with Co–Co bonding and a correct level occupation pattern for a formal Co–Co bond order of 1.5. The half-filled MO (**17**) by symmetry has no wave function density at the bridging PH_2 group and has an overall metal contribution of 80%.

In summary our model calculations for the system $\{[Co(PH_3)_3]_2(PH_2)\}$ with only phosphine ligands at the PH_2-bridged metal centers show that an electronic structure with a singly occupied $a_2(\delta^*)$ Co_2-based orbital and a 1.5 bond order between the metal atoms is only obtained as a consequence of a specific distorted arrangement of the P_6 ligand environment, which is dictated by chelating ligands as employed in the real compound **1**. We note that in particular $PR_2CH_2PR_2$ diphosphinomethane ligands with R = CH_3 can induce the geometric constraints necessary for a stable electronic and molecular structure and that already a replacement of methyl by phenyl or the increased bite size of $PR_2(CH_2)_2PR_2$ diphosphinoethane chelating ligands would probably lead to an electronically unfavorable situation. In line with this result, we did not succeed in preparing an analogue of **1** with bridging $Ph_2PCH_2PPh_2$ ligands instead of $Me_2PCH_2PMe_2$ ligands.

To test this influence further and to eliminate the possibility of an unrealistic electronic structure description of **1** due to our model with only terminal phosphine ligands, we have also performed MO calculations for **18**, the parent system of **1** (H substituted for Me) with a geometry adapted from the X-ray data of **1** and with an idealized C_{2v} overall geometry. Both chelate

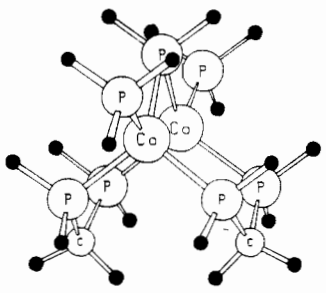

18 (● = H)

rings of **18** have been kept in chair conformations to allow for overall C_{2v} symmetry. This slightly idealized input geometry is plotted in **18**. The resulting upper levels for **18** are also given in Figure 6 on the right side. Again the a_2-type (δ^*) SOMO is found, while the MO corresponding to $4a_1$ lies at lower energy and is doubly occupied. The overall picture is identical with that for the simplified $Co_2(PH_3)_6$ model with enforced chelatelike P_6 framework. The Co–Co overlap population is 0.147 in **18**. A slight difference in comparison to the PH_3 carrying system in the middle of Figure 6 lies in the somewhat smaller energy gap between the SOMO $2a_2$ and the next filled levels $4a_1$ and $2b_1$.

All experimental observations described for $\{[(Me_2PCH_2PMe_2)(PMe_3)Co]_2(PMe_2)\}$ (**1**) are in accord with the electronic structure description of **18**. The unpaired electron resides in a metal-based level that, by symmetry, has no wave function contribution and spin density at the μ-phosphido group and is Co–Co δ antibonding. It is understandable that a reversible one-electron reduction to $\mathbf{1}^-$, a closed-shell anionic system, is readily possible: the extra electron goes into $2a_2$, diminishing the metal–metal bond order but, due to the δ^* character of this orbital, not breaking the Co–Co bond. An elongated Co–Co bond length should be found for $\mathbf{1}^-$. Further reduction to a persistent dianion would require filling $4b_2$ with one electron, and this is clearly an energetically too costly and destructive event to occur and thus is not found experimentally. On the other hand, as oxidation of **1** to $\mathbf{1}^+$ removes the single electron from $2a_2$, the resulting closed-shell cation $\mathbf{1}^+$ should have a somewhat shortened Co–Co bond (formal bond order of 2) and an experimental structural comparison of isolated $\mathbf{1}^+$ (see above) and **1** should provide a direct test of the nature of the half-filled MO of **1**. Note that the nature of $2a_2$ predicts also that neither reduction to $\mathbf{1}^-$ nor oxidation to $\mathbf{1}^+$ should affect the Co–PMe_2 bonds much.

Further oxidation of $\mathbf{1}^+$ to $\mathbf{1}^{2+}$ and to $\mathbf{1}^{3+}$ will remove one and two electrons, respectively, from the next group of levels below $2a_2$. These oxidation steps are found in the CV experiments, but the resultant level occupation pattern for $\mathbf{1}^{2+}$ ("Co_2^{3+}") and $\mathbf{1}^{3+}$ ("Co_2^{4+}") cannot be safely deduced from the MO level scheme of **18**, because it seems unreasonable to simply assume unchanged geometries for these higher charged species. No geometry optimizations for any of the anionic or cationic models **18** were performed, but we think that for both the diamagnetic anion $\mathbf{1}^-$ and for the diamagnetic cation $\mathbf{1}^+$ the assignment of one electron added to or removed from the $2a_2$ orbital and of a retained geometry as in **1** and **18** is valid.

Naturally our conclusion, that it is the specific function of the two chelating small $Me_2PCH_2PMe_2$ ligands to stabilize **1** compared to analogous and isoelectronic $Co_2P_6(\mu\text{-}PR_2)$ molecules (P = monodentate phosphine), leads us to Cowley's compound **2** and its simplified model **11**. Here no geometric constraint can hamper the relaxation of the $Co(CO)_3$ groups. Again, however, the ESR investigation shows only coupling of the unpaired electron to two equivalent Co centers and no coupling to the PR_2 bridge, suggesting an electronic structure analogous to that of **1**. As for **10**-cis and **10**-trans we therefore performed geometry optimizations also for **11**-cis and **11**-trans (angles α, β, and γ defined as before, Co–C–O kept linear throughout). Here the two optimum geometries of **11**-cis (α = 159.5°, β = 93°, γ = 110°) and **11**-trans (α = 90°, β = 124°, γ = 110°) differ by only 5 kcal, favoring **11**-cis. Note that the tiny energetic difference is indicative of facile $Co(CO)_3$ group rotations and fluxional character. A conformational choice in the solid state (should structure determination of a $[(CO)_3Co]_2PR_2$ molecule become available) may therefore depend strongly upon the steric requirements of the PR_2 group and crystal-packing forces and may differ for different PR_2 bridges. If one compares the relaxed structure computed for **11**-cis with the analogous minimum structure of **10**-cis of the system $[(PH_3)_3Co]_2PH_2$ or both trans configurations with each other, the reorientation of each $Co(CO)_3$ group of **11** is much more pronounced than that found for the $Co(PH_3)_3$ groups in **10**. The linear CO ligands allow for a stronger "tilting" of the CoL_3 groups than do the sterically more demanding PH_3 (or any PR_3) ligands. For the $Co_2(CO)_6$ fragment in **11** the minimum structure of **11**-cis comes close to the P_6-frame geometry in the previous chelate model of $[(PH_3)_3Co]_2PH_2$ and to **18** or **1**, respectively; even α is larger. Structure plots for optimized **10**-cis, chelate-modeling **10**-cis, **18**, and optimized **11**-cis in directly comparable orientations are shown for comparison in Figure 7. Therefore, it is not surprising that for both **11**-cis and **11**-trans minima the calculations predict the unpaired electron to be again in a δ^*-type MO of a_2 symmetry. The electronic structure difference between systems **10** with PH_3 and **11** with CO ligands, however, not only is a consequence of a stronger relaxation of the Co_2L_6 skeleton in the sterically less demanding carbonyl case but also has an electronic component.

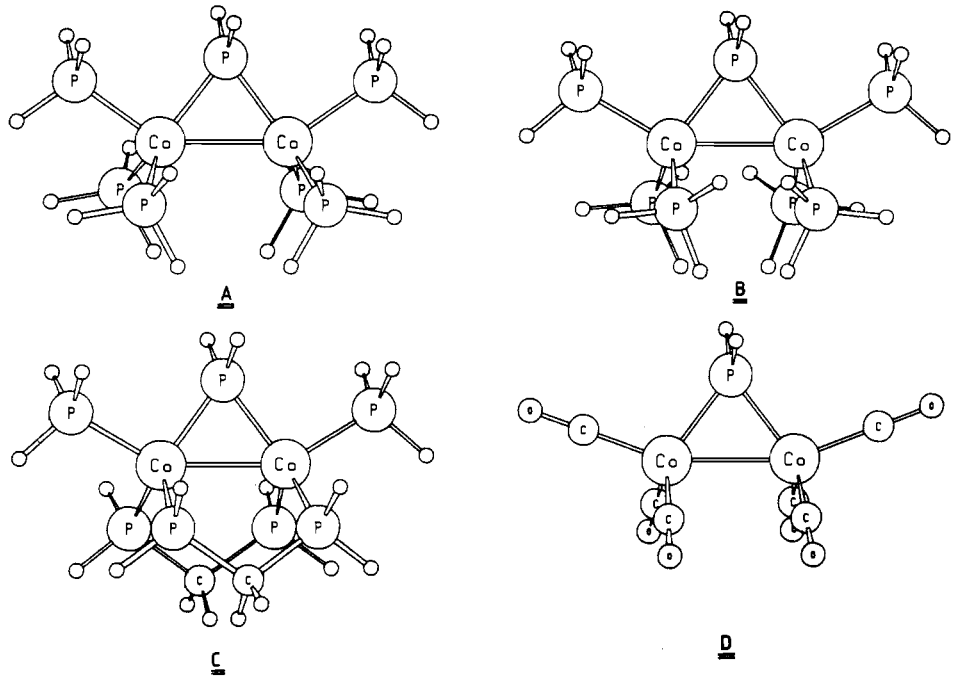

Figure 7. Structural representations of (A) **10**-cis with optimized geometry, (B) **10**-cis modeling **1**, (C) **18**, and (D) optimized **11**-cis.

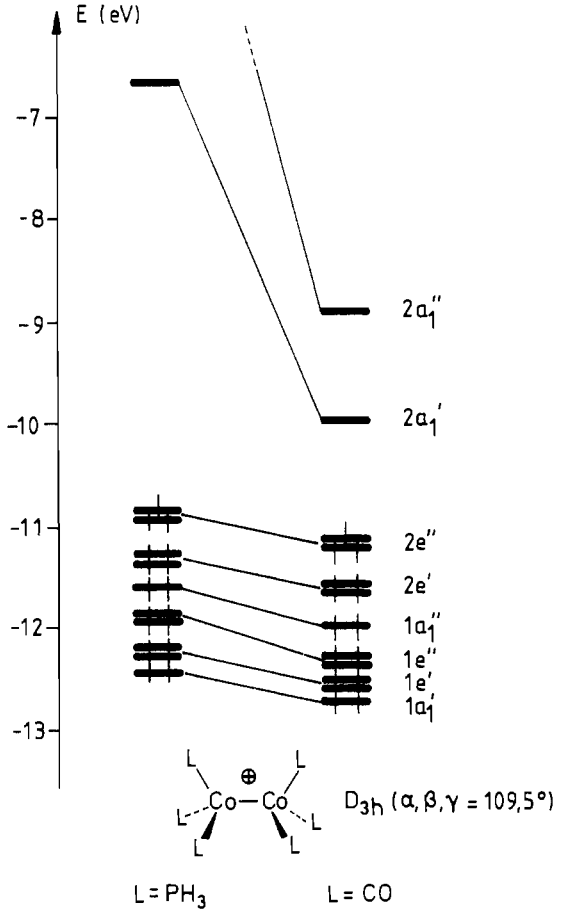

Figure 8. Comparison of valence MOs for D_{3h} fragments $Co_2(PH_3)_6$ and $Co_2(CO)_6$.

The orbital structure of a D_{3h} or "sawhorse" (C_{2v}) $Co_2(CO)_6$ fragment and its bonding capability toward bridging ligands in $M_2(CO)_6$(ligand) complexes have been discussed by Thorn and Hoffmann[21] in detail, and we only show the MOs of D_{3h} $Co_2(PH_3)_6$ and D_{3h} $Co_2(CO)_6$ for the sake of comparison in Figure 8.

An interaction diagram with a PH_2 bridging group is very similar to that of Figure 4, and the relevant differences are easy to understand. Due to the acceptor character of the CO ligands all d-based levels are stabilized. The most pronounced stabilization and descent in energy, however, is experienced by the $2a_1'$ level, the bonding combination of the two CoL_3 sp-hybrid MOs, and by its antibonding counterpart, $2a_1''$, which for $Co_2(PH_3)_6$ was too high in energy to be shown in Figure 4. If we refer back to the latter interaction diagram, it is obvious, then, that the low energy of $2a_2''$ and $2a_1'$ for the $Co_2(CO)_6$ case will keep MOs corresponding to $4b_2$ and especially $4a_1$ of the composite system at lower energy than in the PH_3 case, by mixing in from above in a bonding way as already shown for $4a_1$ in **12**. Our calculations for a $Co_2(CO)_6(PH_2)$ model with a D_{3h} metal fragment indeed place $4a_1$ close in energy above the $2a_2$-type level even for this unrelaxed model geometry. Geometry optimization toward e.g. the minimum structure of **11**-cis for the same (steric) reasons as discussed in the case of **10** therefore pushes $4a_1$ down into the d manifold, leaving $2a_2$ as the SOMO. Again relaxation toward the best geometry of **11**-cis (and **11**-trans) reorients the two lobes of $2a_1'$ as shown in **15**; now its stabilizing interaction with $n(a_1)$ of PH_2 is much stronger due to the low energy of $2a_1'$. In a simplified description the relaxation toward the minimum structures of **11** or the enforced chelate geometry of **18** (and of its model with PH_3 ligands) replaces repulsive interactions of $n(a_1)$ of PH_2 with d levels by bonding of $n(a_1)$ to the two sp hybrids of $2a_1'$ of Co_2L_6 and puts the single electron into the least antibonding (actually nonbonding) d level of the metal fragment. The small energetic difference that is favoring geometry **11**-cis over **11**-trans by about 5 kcal/mol may be traced back to the somewhat different overlap situations leading to a different appearance of $2a_2$ and of $4a_1$. $2a_2$, the SOMO, is less antibonding, more δ^*, for **11**-cis than for **11**-trans, as indicated in **19** vs. **20**, and therefore appears at lower energy. $4a_1$ is more Co–Co bonding and less

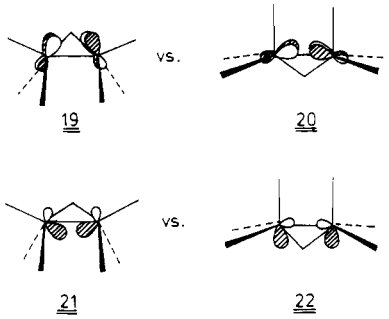

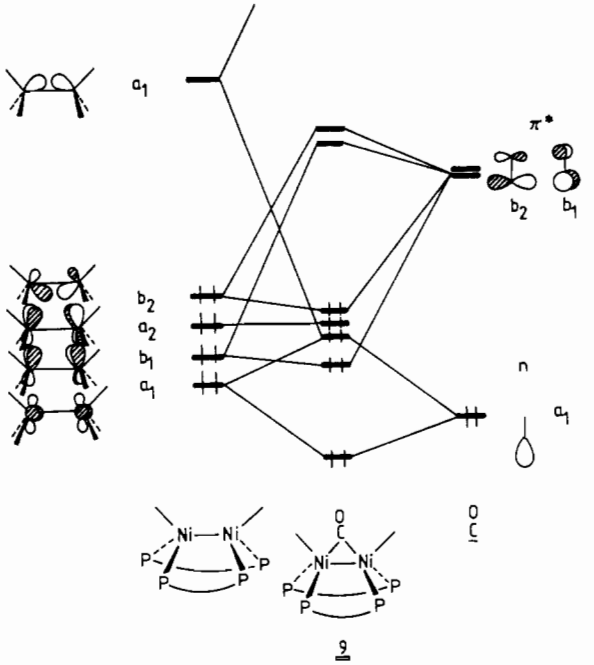

9

Figure 9. Interaction diagram for the CO-bridged nickel dimer **9** (simplified; the d-based levels of the dimetal fragment that are not affected much by the bridging CO being omitted).

Co–PH_2 antibonding in **11**-cis compared to the case in **11**-trans and therefore also more stabilized in the former; cf. **21** vs. **22**. Similar to the case of other closed-shell $Co_2(CO)_6$(ligand) complexes,[21,22,25] for instance $Co_2(CO)_6$(acetylene), $4a_1$ of **11**-cis (**21**) represents the "bent metal–metal bond" and is essentially Co–P nonbonding. The δ^* level $2a_2$ (**19**) for such complexes holds two electrons; for the analogous $Fe_2(CO)_6$ complexes with two electrons less it is empty, leading to a shorter M–M bond, as discussed elsewhere.[21]

Nothing is known to us about the redox behavior of Cowley's compound **2**; it should be possible to reduce it by one electron, thus filling $2a_2$ with concomitant lengthening of the Co–Co bond of the anion $\mathbf{2}^-$ formed. Oxidation analogous to $\mathbf{1} \rightarrow \mathbf{1}^+$ may be possible but will probably weaken the Co–CO bonds considerably, so that the diamagnetic cation $\mathbf{2}^+$ may be rather unstable.

Undoubtedly in compound **2** with $P[CH(SiMe_3)_2]_2$ instead of PH_2 steric shielding by the large PR_2 group enhances kinetic stability and the chelate rings of **1** certainly play a similar role.

In summary, from our model calculations for **1** and **2** we can conclude that such $[CoL_3]_2(\mu\text{-}PR_2)$ radicals (Co_2^+, d^8–d^9) will have a Co–Co bond (of formal bond order 1.5) as well as a δ^*-type SOMO with the nonbonding, unpaired electron delocalized over both metal centers but not in the PR_2 bridge, if the Co_2L_6 fragment can adopt a sufficiently relaxed geometry to ensure an MO sequence of $2a_2$ above $4a_1$. This is the case for CO ligands but not, however, for the monodentate phosphines PR_3. Only the small bite size of chelate ligands of the diphosphinomethane type allows us to reach the required MO pattern in W-frame compounds like **1**. It will be interesting to see whether similar paramagnetic complexes with other three-atom-bridge ligands will be made.

(25) (a) Hoffmann, D. M.; Hoffmann, R.; Fisel, C. R. *J. Am. Chem. Soc.* **1982**, *104*, 3858–3875. (b) Ban, M. I.; Revesz, M.; Balint, I.; Varadi, G.; Palyi, G. *THEOCHEM* **1982**, *88*, 357–370. (c) Anderson, A. L.; Fehlner, T. P.; Foti, A. E.; Salahub, D. R. *J. Am. Chem. Soc.* **1980**, *102*, 7422–7429.

Table IV. Extended Hückel Parameters

orbital		H_{ii}, eV	exponents[a] ζ_1	ζ_2
Co	4s	−8.54	2.0	
	4p	−4.76	2.0	
	3d	−12.11	5.55 (0.5678)	2.10 (0.6058)
P	3s	−18.60	1.60	
	3p	−14.00	1.60	
C	2s	−21.40	1.625	
	2p	−11.40	1.625	
O	2s	−32.30	2.275	
	2p	−14.80	2.275	
H	1a	−13.60	1.30	

[a] Two Slater exponents are listed for d functions. Each is followed in parentheses by its coefficient in the double-ζ expansion.

Finally we comment briefly upon the electronic structure of a diamagnetic nickel dimer with a CO bridge, **9**. Here, according to the partial and qualitative interaction diagram of Figure 9 (both fragments counted neutral, only the relevant MOs shown) the metal fragment $Ni_2(PH_3)_6$, which binds CO, carries three electrons more and the bridging CO ligand instead of a filled b_2 MO like PH_2^- offers an empty π^*_{CO} MO of the same symmetry. A nice closed-shell MO pattern with a large HOMO–LUMO gap arises; a net metal–metal bonding interaction is still present, because $4a_1$ is filled, $3b_2$ is partially depopulated, and the bonding sp hybrid combination of the Ni_2 fragment is populated by $n(a_1)$ of CO.

Acknowledgment. We are indebted to Dr. J. Pebler, Marburg, West Germany, for the magnetic measurements and to Dr. F. R. Kreissl for the mass spectrum of **1**. We also thank Dr. G. Müller and J. Riede for their assistance in processing the X-ray data. Financial support from the Deutsche Forschungsgemeinschaft and the Fonds der Chemischen Industrie (P.H., H.H.K.) is gratefully acknowledged. Support of this work was also generously provided by the Robert A. Welch Foundation (T.A.A.) and the Scientific Affairs Division of NATO (T.A.A., P.H.). T.A.A. is also grateful for a Camille and Henry Dreyfus Teacher-Scholar grant (1980–1984) and an Alfred P. Sloan Research Fellowship (1982–1984).

Appendix

All extended Hückel calculations[20] with the atomic parameters listed in Table IV have been performed with use of a modified Wolfsberg–Helmholtz formula.[26] The following geometric parameters were used: Co–Co = 260 pm, Co–P = 214 pm, P–H = 142 pm, P–C = 184.8 pm, Co–C = 180 pm, C–O = 114 pm, C–H = 110 pm; PH_3-groups, H–P–H = 109.5°; μ-PH_2 group, H–P–H = 110°; Co–C–O = 180°; H–C–H = 109.5°. For other details see text.

Registry No. **1**, 79101-54-5; $\mathbf{1}^-$, 104014-02-0; $\mathbf{1}^+$, 104014-01-9; $\mathbf{1}^{2+}$, 104014-03-1; $\mathbf{1}^{3+}$, 104014-04-2; **2**, 104014-05-3; **9**, 51391-40-3; **10**-cis, 104014-06-4; **10**-trans, 104069-07-0; **11**-cis, 104014-07-5; **11**-trans, 104069-08-1; **18**, 104014-08-6; $[(Me_3P)(Me_2PCH_2PMe_2)_2Co]Cl$, 85752-26-7; $(PMe_3)_2(Me_2PCH_2PMe_2)CoCl_2$, 78856-94-7; $(Me_3P)_3CoCl$, 55516-89-7; $(Me_3P)_4Co$, 33152-37-3; $(Me_3P)_3CoCl_2$, 77209-26-8; Co, 7440-48-4.

Supplementary Material Available: Tables of positional and thermal parameters of the hydrogen atoms and additional distances and angles for **1** (4 pages); a table of observed and calculated structure factors for **1** (6 pages). Ordering information is given on any current masthead page.

(26) Ammeter, J. H.; Bürgi, H.-B.; Thibeault, J. C.; Hoffmann, R. *J. Am. Chem. Soc.* **1978**, *100*, 3686–3692.